Journal of Power Sources 208 (2012) 434–439

Contents lists available at SciVerse ScienceDirect

Journal of Power Sources

journal homepage: www.elsevier.com/locate/jpowsour

Cu–$Si_{1-x}Ge_x$ core–shell nanowire arrays as three-dimensional electrodes for high-rate capability lithium-ion batteries

Jiazheng Wang, Ning Du, Hui Zhang, Jingxue Yu, Deren Yang*

State Key Laboratory of Silicon Materials and Department of Materials Science and Engineering, Zhejiang University, Hangzhou 310027, People's Republic of China

ARTICLE INFO

Article history:
Received 15 December 2011
Received in revised form 9 February 2012
Accepted 13 February 2012
Available online 22 February 2012

Keywords:
SiGe
Three-dimensional electrodes
Anode
Lithium-ion batteries

ABSTRACT

We demonstrate the synthesis of new Cu–$Si_{1-x}Ge_x$ core–shell nanowire array electrodes by directly depositing $Si_{1-x}Ge_x$ layer on the surface of pre-synthesized Cu nanowire arrays via co-sputtering method. When used as anodes of lithium-ion batteries, the Cu–$Si_{1-x}Ge_x$ ($x = 0.4$) nanowire array electrodes show excellent electrochemical performance in terms of cycle stability and rate capability, which is much better than that of planar electrodes. The improved performance can be attributed to the good strain accommodation, fast electron transport and good electrical contact of the nanowire array electrodes. The effect of Ge content and the thickness of alloy film on the electrochemical performance of the three-dimensional electrodes have also been investigated.

1. Introduction

Lithium-ion batteries are currently vital power sources for a variety of modern portable electronic devices and have also promising potential applications in electric vehicles or power tools [1–3]. At present, graphite is used as the commercial anode material for lithium-ion batteries, however, it has a relatively low theoretical capacity (372 mAh g^{-1}) which greatly limits its further application in the next-generation lithium-ion batteries [4]. Therefore, searching new electrode materials with high energy density and high-rate tolerance has attracted great interest [5–8].

Group IV elements (Si, Ge, Sn, Pb) are believed to be ideal candidates for anode materials with respect to high storage capacity. Among them, Si is most appealed because it has the highest known theoretical charge capacity and is the abundant reserves in earth [9]. Various forms of Si electrode materials have been tried, including Si nanowires, thin films, Cu–Si core–shell nanowire array and 3D porous particles [10–13]. However, they are still not satisfactory because the slow kinetics of lithium transport in silicon results in the poor rate capability, which limits their application in high-temperature and high-rate lithium-ion batteries. Comparing to Si, Ge shows a relatively low capacity of 1600 mAh g^{-1} when exhibiting a $Li_{21}Ge_5$ alloy [14]. However, the diffusivity of lithium ions in Ge is much higher (400 times) than that in Si at room temperature, which can lead to high-rate capability [15]. From this point of view, the alloy Si with Ge may improve the diffusivity of lithium ions in silicon, which ultimately improve the rate-capability of anode materials for lithium-ion batteries.

It is reported that an electrode based on alloy material still suffers from poor performance owing to large volume change during the charge and discharge process, which leads to a loss of electrical contact and eventual fading of capacity [16]. Several strategies have been proposed to improve the cyclability of alloy materials, including such as using superfine alloy, intermetallic compounds and active/inactive composite alloy materials [17–19]. These approaches can only improve the electrochemical performance of the alloy anodes to a limited extent. Recently, significant improvements in battery performance were obtained using ordered active nanostructures grown directly on current collector substrates as anode. For example, Taberna et al. reported a nano-architectured Fe_3O_4 anode for lithium-ion batteries, which delivered long cyclic life and good power performance [20]. Scrosati and co-workers have prepared the 3D Ni–Sn nanostructured electrode by electrodeposition of NiSn layer onto Cu nanorods, which exhibits stable cycling capacity (500 mAh g^{-1}) [19]. It is believed that the improved performance and high rate capability is attribute to the efficient buffering of the volume change, fast electron transport and good electrical contact of the order-aligned nanostructure.

Herein, we introduce a Cu–$Si_{1-x}Ge_x$ core–shell three-dimensional electrode and demonstrate its meaningful improvement in cycling life and power rate capability for lithium-ion batteries. The effect of Ge content and the thickness of alloy film on the electrochemical performance of the three-dimensional electrodes have been investigated.

* Corresponding author. Tel.: +86 571 87951667; fax: +86 571 87952322.
E-mail address: mseyang@zju.edu.cn (D. Yang).

0378-7753/$ – see front matter © 2012 Elsevier B.V. All rights reserved.
doi:10.1016/j.jpowsour.2012.02.039

2. Experiment

2.1. Synthesis of Cu nanowire arrays on Cu substrate

Briefly, Cu nano-architectured arrays on Cu substrates were fabricated by the cathodic electrodeposition with anodized aluminum oxide (AAO) templates with the pore diameters of about 200–300 nm. Before using the cathode foil, the cathode Cu substrates were mechanically polished with 1.0 μm alpha alumina and 0.25 μm gamma alumina polishing slurry; The electrolyte systems were consisted of $CuSO_4{\cdot}5H_2O$ 100 g L^{-1}, $(NH_4)_2SO_4$ 10 g L^{-1}, diethylenetriamine (DETA) 40 g L^{-1}. The details of synthetic strategy were fully described in the previous paper [20].

2.2. Synthesis of Cu–$Si_{1-x}Ge_x$ three-dimensional electrodes on Cu substrates

$Si_{1-x}Ge_x$ film was deposited on the surface of Cu nanowire arrays by the co-sputtering of a 99.99% pure germanium target and a 99.999% pure silicon target at a working pressure of 3 Pa. The composition of the $Si_{1-x}Ge_x$ film was adjusted by changing the sputtering power of Si and Ge. The substrates were kept at 200 °C. Three types of thickness-controlled $Si_{1-x}Ge_x$ thin films were prepared for comparison by a sputtering time of 15 min, 30 min, 60 min, respectively. The chemical compositions and element distributions of the $Si_{1-x}Ge_x$ electrodes were examined using energy-dispersive spectroscopy (EDS).

2.3. Characterization and electrochemical measurement

The morphology and structure of the obtained samples were examined by scanning electron microscopy (SEM HITACH S4800) with an energy-dispersive X-ray spectrometer (EDX) and transmission electron microscopy (TEM, PHILIPS CM200). Lithium foils and the fabricated core–shell nanowire arrays were used as the electrodes in coin type cells (CR2025) with 1 M $LiPF_6$ in a mixture of ethylene carbonate (EC) and Dimethyl carbonate (DMC) as the electrolyte (EC/DMC, 1:1, v/v). The cells were assembled in a glove box (Mbraun, Labstar, Germany) under an argon atmosphere and aged 12 h before measurements.

A galvanostatic cycling test of the assembled cells was carried out on a Land CT2001A system in the potential range of 1 mV–1.2 V at a discharge/charge current density of 4000 mA g^{-1}. Cyclic voltammetry (CV) was recorded on an Arbin BT 2000 system at a scan rate of 0.1 mV s^{-1}.

The accurate mass of the active material on the Cu-nanoarrays current collector was examined using a microbalance. We measured the masses of bare Cu substrate, the substrate with Cu nanowire arrays and the substrate after sputtering, respectively. Thus, the total masses of the SiGe film could be obtained.

3. Results and discussion

Fig. 1 shows the schematic illustration of the synthetic process for Cu–$Si_{1-x}Ge_x$ core–shell nanowire array-based three-dimensional electrodes. Briefly, a typical synthetic procedure involves in two steps: (1) growth of Cu nanowire arrays on a Cu substrate via the cathodic electrodeposition in an AAO template; (2) deposition of a $Si_{1-x}Ge_x$ layer onto the surface of Cu nanowires by co-sputtering. Fig. 2a shows the scanning electron microscopy (SEM) image of the Cu nanowire arrays. As observed, the uniformly distributed Cu nanowires are well aligned and perpendicular to the Cu substrate with the diameters of about 200–300 nm and the lengths of about 2–3 μm. Fig. 2b and c shows the top and cross-section view SEM images of as-prepared core–shell nanowire arrays with a deposition time of 30 min. It can be seen that the diameters of the nanowires obviously increase and the surface of the nanowires turns to be rough compared to bare Cu nanowires, indicating the formation of $Si_{1-x}Ge_x$ ($x = 0.40$) alloy layer. Transmission electron microscope (TEM) characterization has been performed to further analyze the structure of Cu–$Si_{1-x}Ge_x$ ($x = 0.40$) nanowires. It can be seen from Fig. 2d that a uniform alloy film with the thickness of about 50–80 nm has been deposited onto Cu nanowires, which is consistent with the SEM images. The EDS spectrum in Fig. 2f reveals that the as-prepared samples are composed of the elements of O, Cu, Si and Ge, which may come from the SEM grid and Cu–$Si_{1-x}Ge_x$ core–shell nanowires, respectively.

The electrochemical performance of the Cu–$Si_{1-x}Ge_x$ core–shell nanowire arrays has been systematically measured. Fig. 3a presents the discharge capacity versus cycle numbers for the Cu–$Si_{1-x}Ge_x$ core–shell nanowire electrodes with different Ge contents at a current density as high as 4 A g^{-1}. It can be seen that the initial reversible capacity for the pure Si is about 2142 mAh g^{-1} and dropped to 823 mAh g^{-1} after 75 cycles with a capacity retention of 38.4%, indicating the poor rate capability. When alloyed with 14% Ge, the initial reversible capacity (2074 mAh g^{-1}) decrease due to the relatively low theoretic capacity of Ge, however, the cyclic performance has been enhanced (1121 mAh g^{-1} with 54% retention). The addition of Ge can improve the diffusivity of lithium ions and buffer the volume change during the charge/discharge process, which may explain the enhanced cyclic performance. When the content of Ge increases from 14% to 69%, the capacity retention rates for $Si_{0.86}Ge_{0.14}$, $Si_{0.75}Ge_{0.25}$, $Si_{0.60}Ge_{0.40}$, $Si_{0.43}Ge_{0.57}$, $Si_{0.31}Ge_{0.69}$ are 54.05%, 67.35%, 76.91%, 61.13%, 57.51%, respectively. It can be seen that the capacity retention increases at the initial stage with Ge increases from 14% to 40%, and then decreases when the content of Ge further increases. Previous papers have demonstrated that sputtered $Si_{1-x}Ge_x$ films are amorphous and the increasing content of Ge in the alloy would make the crystallization of the $Si_{1-x}Ge_x$ film easier [21,22]. In addition, it has been reported that the expansion along with lithium insertion in amorphous alloys is homogeneous, while in crystalline materials is inhomogeneous [23]. In this case, some crystalline nanoparticles may be brought during the synthetic process of $Si_{1-x}Ge_x$ alloy when the content of Ge further increases, which induces inhomogeneous volume expansions and cracking of the $Si_{1-x}Ge_x$ alloy electrode. On the other hand, the origin may also relate to the nearly same amount of Si and Ge in the array film. By the difference of alloying/dealloying potentials of Si and Ge with Li, the volume expansion ratio per the potential can be minimized. Besides, surface reactions could be the reason for higher capacity retention for $Si_{0.6}Ge_{0.4}$ alloy anode since there may be some variation for SEI for SiGe at different Ge contents. However, these explanations are preliminary and need further investigation.

According to the optimized retention capacity, the specific capacity of the Cu–$Si_{0.60}Ge_{0.40}$ core–shell nanowire arrays cycled as a function of the cycle number have been tested at a high rate of 4 A g^{-1} at room-temperature (Fig. 3b). It can be seen that the discharge of the first cycle shows a high capacity of about 3954 mAh g^{-1}, which is larger than the theoretical value (3160 mAh g^{-1}). The extra capacity was plausibly attributed to the formation of a surface–electrolyte interphase (SEI) film due to electrolyte decomposition [24,25]. The second discharge and charge capacities were determined as 1958 and 1772 mAh g^{-1}, respectively, giving a Coulombic efficiency up to 91.5% which is much higher than the previous reported Si nanowire electrodes [10]. Moreover, the Coulomb efficiency reached 95.6% at the fifth cycle and kept steadily more than 96% thereafter. Besides, A discharge capacity as high as 1506 mAh g^{-1} after 75 cycles with the retention of about 76.9% can be noticed, indicating the high reversibility of the Cu–$Si_{0.60}Ge_{0.40}$ core–shell nanowire arrays. The rate capability of

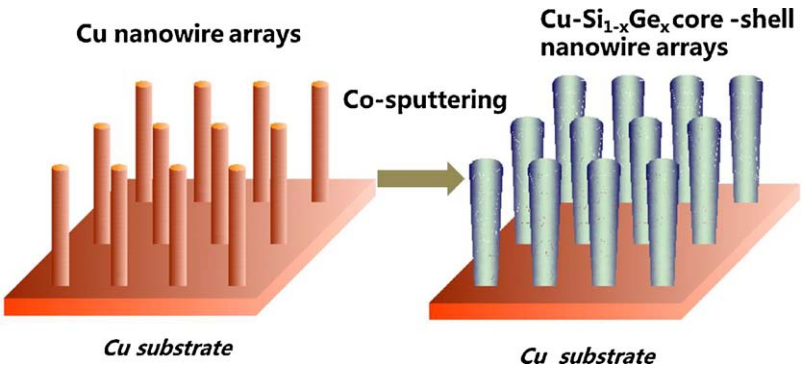

Fig. 1. Schematic illustration for synthesis of a Cu–$Si_{1-x}Ge_x$ three-dimensional electrode.

the three-dimensional electrode has been further studied as shown in Fig. 3c. It can be seen that the Cu–$Si_{0.60}Ge_{0.40}$ core–shell nanowire array electrode reveals the good cyclability at 0.63 C (2 A g^{-1}) with a reversible capacity around 2000 mAh g^{-1} and Coulombic efficiency of 96.2%. With the increased current rate from 1.25 C to 2.5 C and 5 C, the reversible capacities were 1855, 1733, 1592 mAh g^{-1}, respectively. Even at a current density as high as 10 C (32 A g^{-1}), the electrode could deliver a stable capacity of about 1348 mAh g^{-1}. When the current density has been reset to 2.5 C, 99.1% capacity retention could be obtained, indicating the superior rate cyclability of the as-prepared Cu–$Si_{0.60}Ge_{0.40}$ core–shell nanowire electrode.

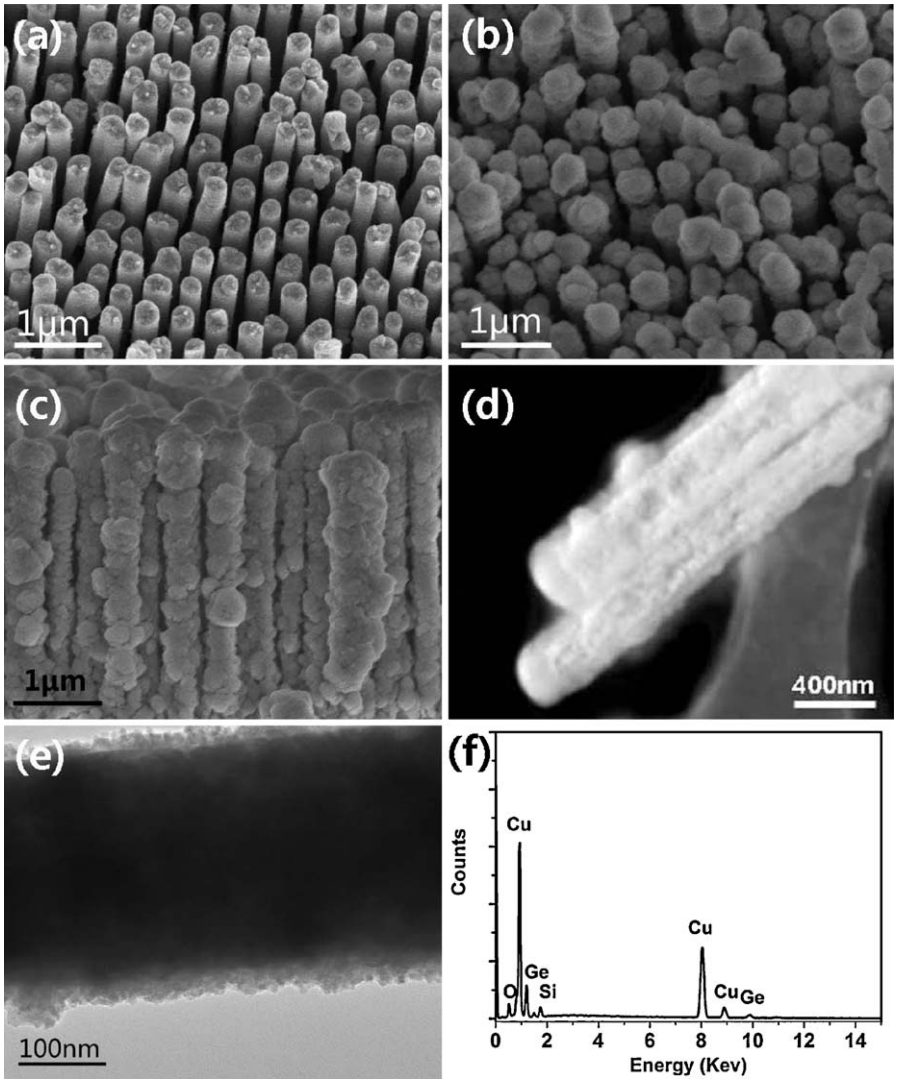

Fig. 2. (a) SEM image of a Cu nanowire array current collector, (b), (c) top-view and cross-section view SEM images of Cu–$Si_{1-x}Ge_x$ ($x = 0.40$) core–shell three-dimensional electrode; (d), (e) STEM and TEM images of Cu–$Si_{1-x}Ge_x$ ($x = 0.40$) core–shell nanowires; and (f) EDX spectrum of the Cu-TEM images of Cu–$Si_{1-x}Ge_x$ ($x = 0.40$) core–shell nanoarrays three-dimensional electrode.

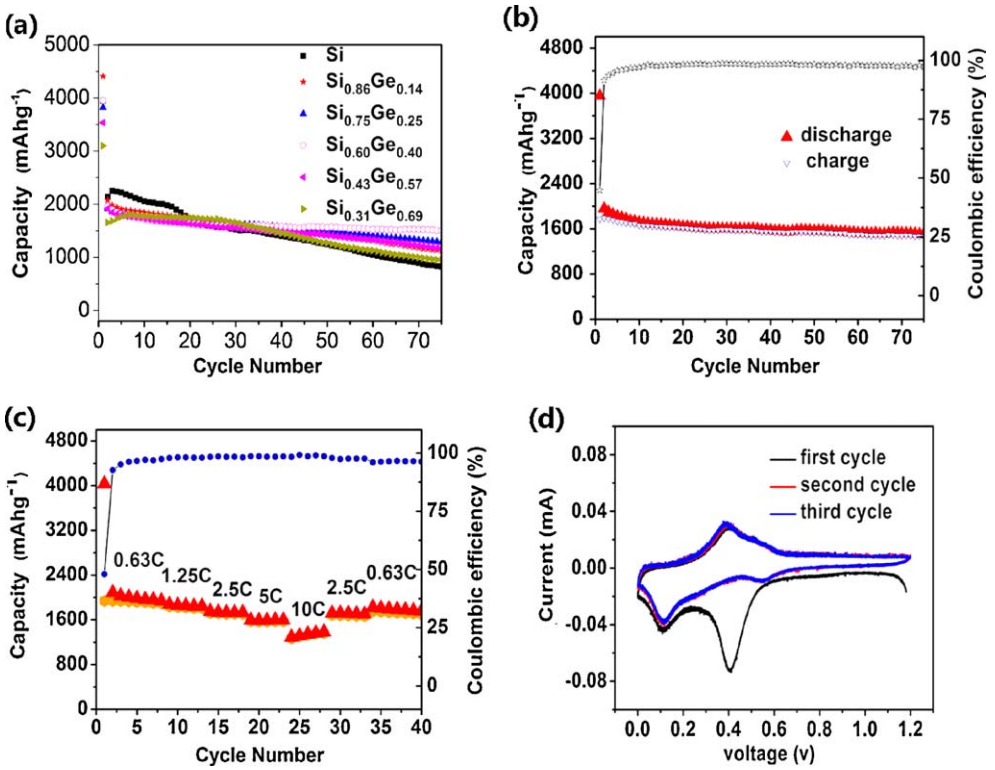

Fig. 3. (a) Cycling performance of Cu–$Si_{1-x}Ge_x$ core–shell nanoarrays three dimensional electrodes with various ratios of Si and Ge; (b) discharge and charge capacities versus cycle number for the Cu–$Si_{1-x}Ge_x$ ($x = 0.40$) core–shell three-dimensional electrode at the rate of 4000 mA g^{-1}; (c) cycling performance at various C rates of the Cu–$Si_{0.60}Ge_{0.40}$ core–shell nanowire three-dimensional electrode; and (d) the first three CV curves of the Cu–$Si_{1-x}Ge_x$ ($x = 0.40$) three-dimensional electrode at a scan rate of 0.1 mV s^{-1} and a temperature of 20 °C.

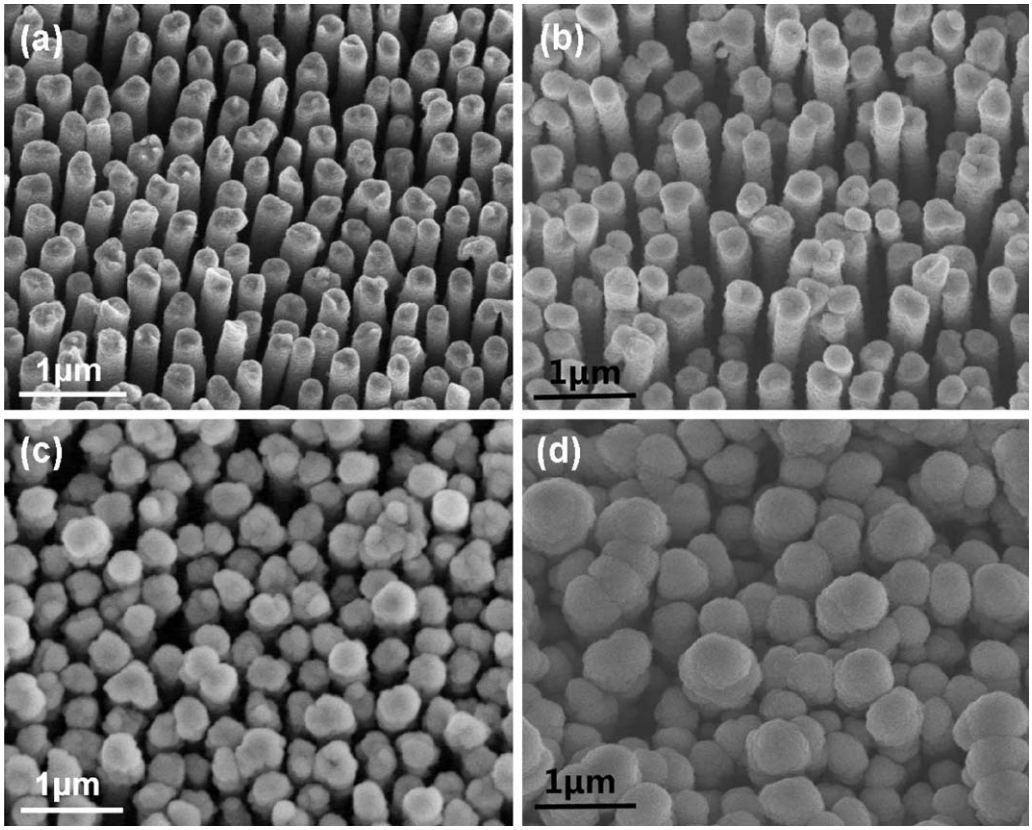

Fig. 4. SEM images of different thickness-controlled $Si_{1-x}Ge_x$ ($x = 0.40$) thin films on cu nanoarray current collectors after deposited $Si_{1-x}Ge_x$ alloy film for (b) 15 min, (c) 30 min, and (d) 60 min, respectively.

Cyclic voltammetry (CV) measurements were carried out to understand the electrochemical reactions during charging and discharging process. The first three CV curves of the Cu–$Si_{0.60}Ge_{0.40}$ nanowire array electrode tested with a scanning rate of 0.1 mV s^{-1} in the potential range of 0–1.2 V is shown in Fig. 3d. During the first discharge (Li alloying) process, the peak locate at the potential of 0.42 and 0.1 V can be attributed to the decomposition of $Si_{0.60}Ge_{0.40}$, the formation of the SEI film and Li_xM (M is Si and Ge) alloy, respectively. In contrast, there are two high current peaks occurring at about 0.39 and 0.50 V in the reduction process. Previous papers have shown that the dealloying reactions of Li–Ge would appear around 0.4 V [4,26], which agree well with the CV results. Anodic peaks at around 0.4 and 0.5 V are attributed to the dealloying reactions of Li–Si [27]. In the second and third cycles, the CV curves show almost no change, suggesting high reversibility of the Cu–$Si_{0.60}Ge_{0.40}$ three-dimensional electrode in the subsequent cycles.

The effects of the thickness of films on the electrochemical performance of Cu–$Si_{1-x}Ge_x$ three-dimensional electrodes have also been investigated. Fig. 4 shows the SEM images of a series of Cu–$Si_{1-x}Ge_x$ ($x = 0.40$) nanowire arrays with different $Si_{1-x}Ge_x$ thickness by adjusting the depositing conditions. It can be seen from Fig. 4b that the surface of the nanowires turns slightly rough with a sputtering time of 15 min compared to the pure Cu nanowire (Fig. 4a), indicating that a thin $Si_{0.60}Ge_{0.40}$ layer may be coated on the surface of the Cu nanowires. When the sputtering time increases to 30 min, the deposited alloy layer becomes denser and thicker (Fig. 4c), suggesting the formation of uniform core–shell structure. If the deposition time is further prolonged to 60 min, the excessive $Si_{1-x}Ge_x$ ($x = 0.40$) film covers on the top of Cu nanowire arrays as observed in Fig. 4d. Cycling performance of the Cu–$Si_{0.60}Ge_{0.40}$ core–shell three dimensional electrodes with different thickness have been tested under the same conditions

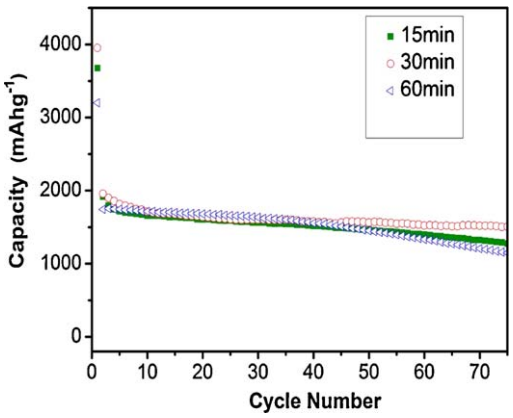

Fig. 5. Discharge and charge capacity versus cycle number of three types of products.

(4000 mA g^{-1}). Fig. 5 exhibits the discharge capacity versus the cycle numbers for the three Cu–$Si_{0.60}Ge_{0.40}$ electrodes with a sputtering time ranging from 15 min to 60 min. It is indicated that the electrode with the sputtering time of 15 min continuously degrades after 75 cycles with a capacity of 1276 mAh g^{-1} since the thinner $Si_{1-x}Ge_x$ ($x = 0.40$) layer may suffer severely from the irreversible surface reaction. For the sample sputtered for 30 min, the electrode shows the excellent cycling stability, which could be explained by the above-mentioned advantages of the nanowire array three-dimensional electrodes. When the depositing time of $Si_{1-x}Ge_x$ ($x = 0.4$) further increases to 60 min, excessive $Si_{1-x}Ge_x$ would cover the top of Cu nanowires, suggesting that there is insufficient space for buffering the volume expansion of electrode during cycling. As a result, the capacity fading is inevitable because this sample

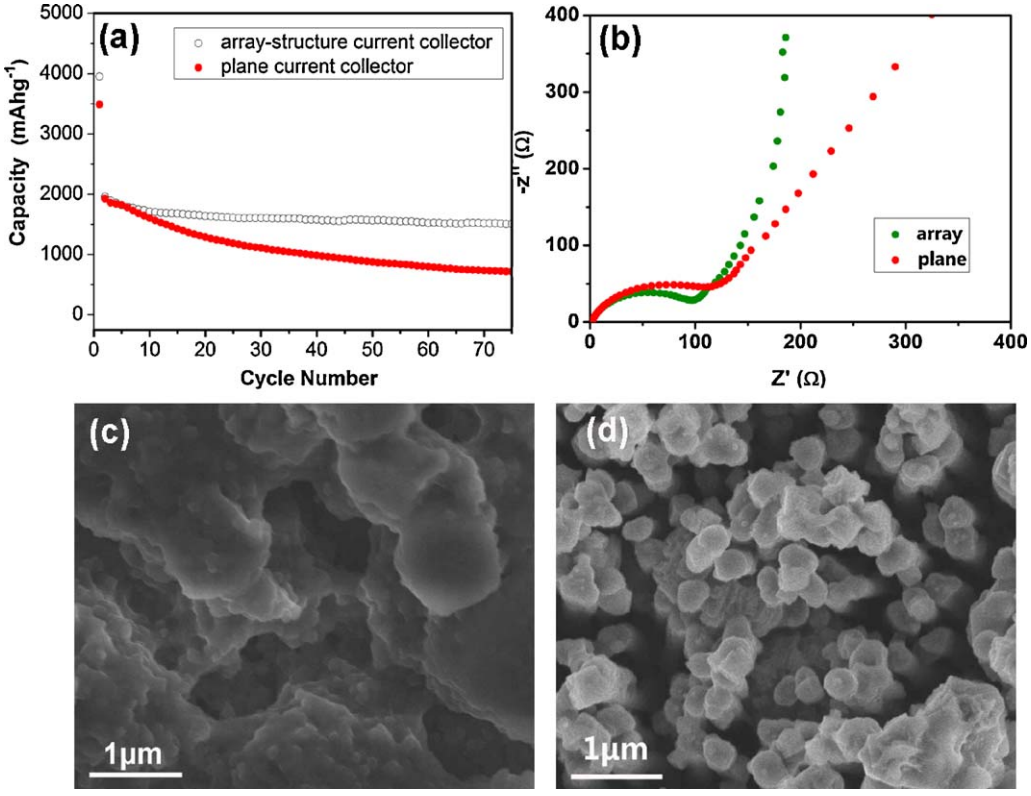

Fig. 6. (a) Cycling performance for the Cu–$Si_{0.60}Ge_{0.40}$ core–shell nanowire array collector and the Cu–$Si_{0.60}Ge_{0.40}$ film on a plane Cu current collector at the current density of 4000 mA g^{-1}; (b) Nyquist plot for plane electrode and three dimensional electrode, respectively; (c) SEM image of the $Si_{0.60}Ge_{0.40}$ film on a Cu substrate after 20 cycles; and (d) SEM image of the Cu–$Si_{0.60}Ge_{0.40}$ three-dimensional electrode after 20 cycles.

fails to take advantage of the merits of the superior array structure efficiently.

In order to intuitively illustrate the advantages of Cu–$Si_{0.60}Ge_{0.40}$ core–shell nanowire arrays as three-dimensional electrodes, electrochemical performance of the three-dimensional electrode and plane electrode have been tested under the same condition for comparison. It can be seen from Fig. 6a that the $Si_{0.60}Ge_{0.40}$ layer on a planar Cu substrate shows the rapid capacity decline and gives a capacity of 715 mAh g^{-1} after 75 cycles. By contrast, the Cu–$Si_{0.60}Ge_{0.40}$ three-dimensional electrode exhibits much larger capacity and better cycling performance than the plane electrode, indicating the advantages of the three-dimensional electrode. The AC impedance measurements (Fig. 6b) were performed on the above-mentioned two electrodes after 5 cycles. All the spectra consist of a depressed semicircle in the high-to-medium frequency range and a straight line in the low frequency range. The charge transfer resistance is responsible for the observed chord of the arc as a consequence of the charge transfer process at the alloy/electrolyte interface. It is clear that the diameter of the semicircle in the Cu–$Si_{0.60}Ge_{0.40}$ three-dimensional electrode is significantly small than that of the plane electrodes, revealing lower charge-transfer impedances. The array-structure leads to a smaller charge transfer resistance and thus reduces the total cell resistance, which leads to the high rate capability Cu–$Si_{1-x}Ge_x$ three-dimensional electrodes. For further identify the advantage of three dimensional electrodes, the SEM analysis of the planar electrode and three-dimensional electrode after 20 cycles were performed (Fig. 6c and d). It can be seen that the three-dimensional electrode maintains the array architecture and no appreciable change in morphology can be noticed, while strong cracks develop over the whole surface of the coating layer in the planar electrode. Therefore, the Cu–$Si_{0.60}Ge_{0.40}$ three-dimensional electrode is considered to be the good stability, good electrical contact, and fast electron transport, which may be responsible for the improved electrochemical performance.

4. Conclusion

In summary, Cu–$Si_{1-x}Ge_x$ core–shell nanowire arrays have been successfully synthesized by directly depositing $Si_{1-x}Ge_x$ layer on the surface of pre-synthesized Cu nanowire arrays via a co-sputtering method. When applied as anode materials of lithium-ion batteries, the composition and thickness of the $Si_{1-x}Ge_x$ layer have been adjusted to optimize the electrochemical performance. The optimized Cu–$Si_{0.60}Ge_{0.40}$ three-dimensional electrode shows a high initial Coulombic efficiency of 91.5% and an initial reversible capacity of 1958 mAh g^{-1} at a current density of 4 Ag^{-1}. After 75 cycles, it delivered a reversible capacity of 1506 mAh g^{-1} with capacity retention of 76.91%. When the Cu–$Si_{0.60}Ge_{0.40}$ three-dimensional electrode has been tested at a higher current density (32 A g^{-1}), it can still deliver a stable capacity of about 1348 mAh g^{-1}. It is believed that the excellent electrochemical performance can be attributed to the good strain accommodation, fast transport of electron and good contact to the current collector of the optimized three-dimensional electrodes.

Acknowledgments

The authors would like to appreciate the financial supports from Innovation Team Project of Zhejiang Province (2009R50005), NSFC (No. 50802086 and No. 51002133) and the Fundamental Research Funds for the Central Universities (Program No. 2011FZA4006).

References

[1] B. Scrosati, Nature 373 (1995) 557–558.
[2] K. Kang, Y.S. Meng, J. Bréger, C.P. Grey, G. Ceder, Science 311 (2006) 977–980.
[3] J.M. Tarascon, M. Armand, Nature 414 (2001) 359–367.
[4] C.K. Chan, X.F. Zhang, Y. Cui, Nano Lett. 8 (2008) 307–309.
[5] N. Du, H. Zhang, B. Chen, J. Wu, X. Ma, Z. Liu, Y.Q. Zhang, D. Yang, X. Huang, J. Tu, Adv. Mater. 19 (2007) 4505–4509.
[6] G.L. Cui, L. Gu, L.J. Zhi, N. Kaskhedikar, P.A. van Aken, K. Mullen, J. Maier, Adv. Mater. 20 (2008) 3079–3803.
[7] J.Z. Wang, N. Du, H. Zhang, J.X. Yu, D.R. Yang, J. Phys. Chem. C 115 (2011) 11302.
[8] Y.X. Wang, L. Huang, Y.Q. Chang, F.S. Ke, J.T. Li, S.G. Sun, Electrochem. Commun. 12 (2010) 1226–1229.
[9] R. Teki, M. Datta, R. Krishnan, T.C. Parker, T.M. Lu, P.N. Kumta, N. Koratkar, Small 5 (2009) 2236–2242.
[10] C.K. Chan, H. Peng, G. Liu, K. McIlwrath, X.F. Zhang, R.A. Huggins, Y. Cui, Nat. Nanotech. 3 (2008) 31–35.
[11] K.L. Lee, J.Y. Jung, S.W. Lee, H.S. Moon, J.W. Park, J. Power Sources 129 (2004) 270–274.
[12] J. Qu, H. Li, J.J. Henry Jr., S.K. Martha, N.J. Dudney, H. Xu, M. Chi, M.J. Lance, S.M. Mahurin, T.M. Besmann, S. Dai, J. Power Sources 198 (2012) 312–317.
[13] Y. Yu, L. Gu, C.B. Zhu, S. Tsukimoto, P.A. van Aken, J. Maier, Adv. Mater. 22 (2010) 2247–2250.
[14] S. Yoon, C.M. Park, H.J. Sohn, Electrochem. Solid-State Lett. 11 (2008) A42–A45.
[15] C.S. Fuller, J.C. Severiens, Phys. Rev. 96 (1954) 21.
[16] W.J. Zhang, J. Power Sources 196 (2011) 13–24.
[17] G.X. Wang, L. Sun, D.H. Bradhurst, S. Zhong, S.X. Dou, H.K. Liu, J. Alloys Compd. 306 (2000) 249–256.
[18] Y.Y. Xia, T. Sakai, T. Fujieda, M. Wada, H. Yoshinaga, J. Electrochem. Soc. 148 (2001) A471–A481.
[19] J. Hassoun, S. Panero, P. Simon, P.L. Taberna, B. Scrosati, Adv. Mater. 19 (2007) 1632–1635.
[20] P.L. Taberna, S. Mitra, P. Poizot, P. Simon, J.M. Tarascon, Nat. Mater. 5 (2006) 567–573.
[21] E.V. Jelenkovic, K.Y. Tong, Z. Sun, J. Vac. Sci. Technol. 15 (1997) 2836–2841.
[22] J. Olivaresa, A. RodrõÂgueza, J. Sangradora, T. RodrõÂgueza, C. Ballesterosb, A. Kling, Thin Solid Films 337 (1999) 51–54.
[23] T.D. Hatchard, J.R. Dahn, J. Electrochem. Soc. 151 (2004) A1628–A1635.
[24] J. Wang, N. Du, H. Zhang, J. Yu, D. Yang, J. Mater. Chem. 22 (2012) 1511–1515.
[25] M. Park, K. Kim, J. Kim, J. Cho, Adv. Mater. 22 (2010) 415–418.
[26] J. Liu, Y. Li, X. Huang, R. Ding, Y. Hu, J. Jiang, L. Liao, J. Mater. Chem. 19 (2009) 1859–1864.
[27] H. Xia, S. Tang, L. Lu, Mater. Res. Bull. 42 (2007) 1301–1309.